Numerical Analysis of Residual Stress Distribution in Tubes with Spiral Weld Cladding

An analysis was conducted to determine the residual stress-strain state in the weld clad tube and verify the developed finite element method

BY B. TALJAT, T. ZACHARIA, X-L. WANG, J. R. KEISER, R. W. SWINDEMAN, Z. FENG AND M. J. JIRINEC

ABSTRACT. Residual stresses and strains in a tube with spiral weld cladding were analyzed by the finite element (FE) method. The objective of this work was to determine the residual stress-strain state in the weld clad tube and verify the developed FE model, which might serve for future parametric sensitivity studies of various welding parameters on residual stresses in such tubes.

An axisymmetric FE model was developed to simulate the circumferential weld cladding process of Alloy 625 on SA210 carbon steel tube and to analyze the residual stress-strain state. The analysis was uncoupled in that the thermal and mechanical analyses were conducted in two separate runs. The results show high tensile residual stresses in the weld cladding and at the interface with a gradual transition to compressive stresses at the inner tube surface.

A neutron diffraction technique was used to experimentally determine residual elastic strains in the clad tube. Comparison with the FE results shows good overall agreement. The agreement is excellent in radial and axial elastic strain components, whereas the calculated tangential elastic strain overpredicted the measured value. The difference is discussed, and certain conclusions are given.

Finally, some attempts on how to prevent or relieve high tensile stresses in the weld cladding are presented and discussed in this paper.

B. TALJAT, T. ZACHARIA, X-L. WANG, J. R. KEISER and R. W. SWINDEMAN are with the Oak Ridge National Laboratory, Metals and Ceramics Division, Oak Ridge, Tenn. Z. FENG is with the Edison Welding Institute, Columbus, Ohio, and M. J. JIRINEC is with Welding Services, Inc., Norcross, Ga.

Introduction

A black liquor recovery boiler is an essential component in kraft pulp and paper mills. It is used to recover certain chemicals and generate process steam by burning the black liquor. The recovery furnace walls are made of water-cooled tubes. Both higher operating pressure, which caused higher wall temperatures, and a highly corrosive environment in the furnace have contributed to rapid corrosion of carbon steel tubes in the lower furnace (floor and lower walls). Type 304 stainless steel was found to be highly resistant to the sulphidizing environment in the boiler; therefore, the composite tubes (304 stainless steel cladding on SA210 carbon steel base tube) were selected to address the corrosion problem (Ref. 1).

Composite tubes in recovery boilers are conventionally coextruded. Several boilers worldwide have experienced extensive cracking in the stainless steel layer after various periods of operation (Ref. 1). A multidisciplinary research program has been initiated to determine the cause of the cracking phenomenon in the stainless steel layer (Ref. 2).

KEY WORDS

Cladding
Alloy 625
Finite Element Analysis
Residual Stresses
SA 210 Carbon Steel
Residual Elastic Strains
Neutron Diffraction

Alternative manufacturing processes are being considered to improve the resistance to cracking and in-service life of composite tubes based on the hypothesis that part of the problem is caused by the tube manufacturing process. Some experience shows that floor sections repaired with corrosion-resistant welds are more resistant to cracking than the neighboring coextruded composite tubes. Consequently, circumferentially welding the corrosion-resistant cladding, typically Alloy 625 or Type 309 stainless steel, on carbon steel tubes (SA210 Grade A1 carbon steel) is being considered as an alternative manufacturing process, and was studied in this work.

In general, the physics of a welding process are very complex. The welding arc produces very high temperatures, instantaneously melting the material in its vicinity. The heat input is defined by welding parameters that, combined with heat losses, are functions of the type of materials used, geometry and size of the workpiece and fixturing; they determine the fusion-zone size and the intensity of thermal gradients during cooling. The intensity of thermal gradients during cooling influence the deformation patterns, which finally produce the residual stress distribution in the product. Various types of welding processes have been successfully modeled by finite element (FE) analysis to determine welding residual stresses (Refs. 3–6).

The objective of this study was to analyze the residual stress state after the welding process; this evaluation is important for a successful study of the stress conditions during operation of a boiler. The in-service stresses are a crucial factor because they can either assist or prevent the initiation and/or propagation of cracks under various mechanisms, such as stress-corrosion cracking, thermal fatigue, or a combination of these.

Fig. 1 — Tube with a spiral cladding.

An axisymmetric FE model was developed to simulate the weld cladding process performed in two layers – gas metal arc welding (GMAW) for the first layer and gas tungsten arc welding (GTAW) for the second layer. Thermal and mechanical analyses were performed using ABAQUS FE code (Ref. 7). Part of this work included verification of the developed FE model. Consequently, neutron diffraction (ND) was used to measure residual elastic strains in an as-manufactured tube (Ref. 8), and the results were used for comparison with the FE results. The comparison is very promising for future FE studies of residual stresses in weldments. The developed FE model might be useful in future sensitivity studies analyzing the effect of welding parameters on the residual stress distribution.

Some approaches also were considered to prevent or reduce high tensile residual stresses in the weld cladding. Heat treatment of the weld clad tube after the welding is one approach and changing some welding parameters is another. The results of both processes are presented and discussed in this paper.

Overview of the Welding Process

The welding process consists of two layers continuously applied in the circumferential direction, resulting in a spiral 360-deg weld cladding — Fig. 1. The first layer is made with a single electrode (~1-mm-diameter) by the automated GMAW process with filler material, and the autogenuous GTAW process is used to make the second layer. The purpose of the second layer is to temper the heat-affected zone. The width of the weld bead is approximately 9 mm, which indicates that a special welding technique — electrode weaving — is used to achieve the desired weld width. The tube is water-cooled during welding, and preheat is not applied. Table 1 shows the welding parameters adequate for modeling.

Neutron Diffraction Measurements

The ND measurements were conducted separately in a parallel study. Because details of the experiment have been reported elsewhere (Ref. 8), only an outline is given here. Basically, this method uses one or more diffraction peaks as a strain sensor. From the measured diffraction peak position, the interplanar lattice spacing is obtained. The lattice strain is then determined using the equation,

$$\varepsilon = \frac{d - d_0}{d_0} \qquad (1)$$

where d_0 is the unstressed lattice spacing. In this study, d_0 for each material was obtained by measuring a stress-free reference specimen, prepared using a part of the supplied weld clad tube (Ref. 8).

The incident and diffracted beams were defined, respectively, by masking slits inserted before and after the specimen. The intersection of the incident and diffracted beams formed the sampling or gauge volume. Strain mapping was accomplished using a three-dimensional translation stage mounted on the sample table of the neutron diffractometer. All ND measurements were performed at the High Flux Isotope Reactor of Oak Ridge National Laboratory (ORNL).

Note that the slits used for radial and tangential strain measurements are 30 mm long, whereas 4-mm-long masking slits are used for axial strain measurements. This indicates that the measured strains in the radial and tangential directions represent an average across several weld passes, which is an important factor to keep in mind when the ND results are compared with FE calculations. Also, to ensure that the obtained strain values are representative, the radial and hoop strain profiles were determined at several locations around the tube, and the results were averaged. The axial strain was measured at only one angular position because of the small sampling volume. Therefore, long counting time was required for this measurement geometry.

Finite Element Analysis

Complex numerical models are required to thoroughly model the physics of this welding process. In the thermal analysis one should account for 1) conductive and convective heat transfer in the weld pool, 2) convective, radiative and evaporative heat losses at the weld pool surface, and 3) heat conduction into the surrounding solid material, as well as the conductive and convective heat transfer to the ambient through cooling substances surrounding the tube. Furthermore, one needs to account for temperature-dependent material properties, the effect of latent heat of fusion, as well as the material phase transformation effects. Capturing all of these effects results in a complex FE model. However, some effects may considerably complicate the analysis and yet have negligible effects on the final result. Therefore, one's best judgment should be used in such cases to decide on simplifications and assumptions for establishing an effective and yet reasonably accurate FE model.

An axisymmetric model was considered because of the circumferential welding direction. This assumption considerably simplifies the modeling effort and reduces the computational time. However, it requires acceptance of addi-

Table 1 — Welding Parameters

	Layer 1	Layer 2
Welding technique	GMAW	GTAW
Welding current [A]	170–200	360–400
Welding voltage range [V]	20–25	9–12
Travel speed [mm/s]	12–13	12–13
Electrode diameter [mm]	1.2	3.2
Weave width [mm]	9–12	9–12
Weld bead width [mm]	9–10	9–10

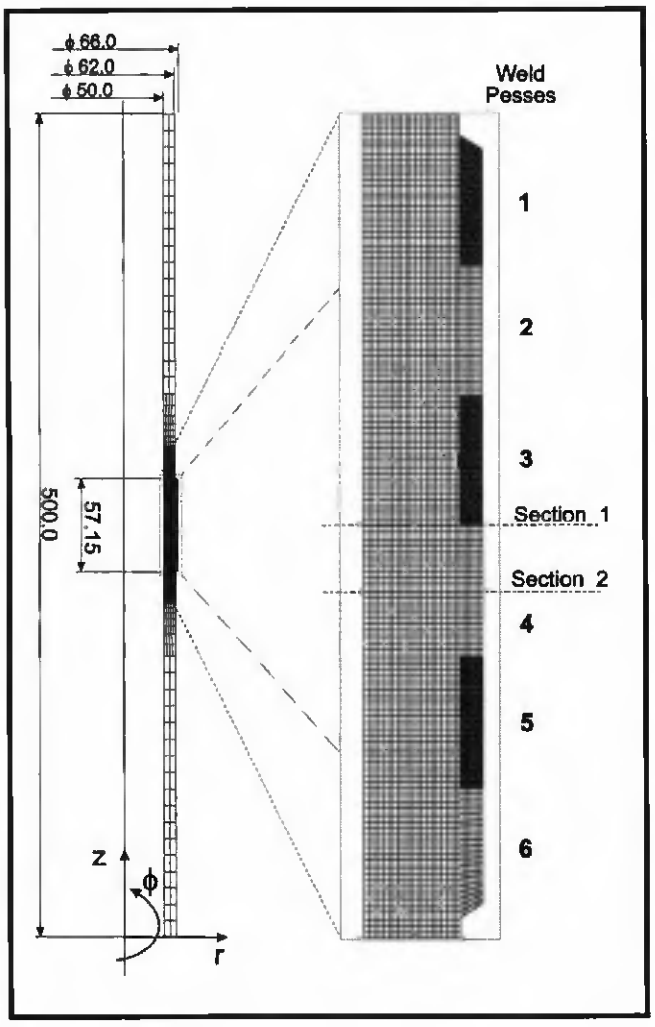

Fig. 2 — FE model.

Table 2 — Tube Cooling Parameters

Water flow rate [cm³/s]	946–1892
Prandtl number, Pr	7.049
Reynolds number, Re	25104 ÷ 50208
Tube-water convection coefficient, h_f [W/m² K]	2984
Tube-air convection coefficient, h_a [W/m² K]	10.0

tional assumptions, which mainly address how heat is introduced into the model.

The overall tube length considered in the model is 500 mm, which is approximately nine times the length of the weld cladding considered in the analysis. The reason for selecting this tube length is to appropriately model the conductive, convective and radiative heat transfer during welding. Changing the tube length affects the intensity of the thermal sink (cooling water) and thus the steady-state temperature of the tube during welding. The model length was therefore selected on the basis of the calculated temperature, not exceeding 40°C (104°F) at a particular distant point on the tube.

Figure 2 shows the FE model, essential dimensions and some mesh details, in addition to the sections from which the residual stress results are presented.

Computations were performed using ABAQUS FE code. The core of the modeling effort is in the user subroutines for ABAQUS code, which allow the simulation of the welding arc movement over the material. Thermal and mechanical analyses are uncoupled and performed in two separate runs. First, the thermal analysis is performed calculating the transient temperature distributions during welding. The model for the mechanical analysis is similar to the thermal one, except for the type of finite elements and the applied boundary conditions. The mechanical part relies on the thermal analysis results and calculates the stress-strain distribution on the basis of the temperature gradients.

Thermal Analysis

Several assumptions and simplifications were made in the thermal model. The welding arc was modeled by a heat flux moving across the observed section of the tube. Electrode weaving was not modeled; instead, a wider heat flux was assumed, which corresponds to the weld bead width. To account for heat transfer effects due to fluid flow in the weld pool, an increase in the thermal conductivity above the melting temperature was assumed. The phase transformation effect was modeled by specifying the latent heat of fusion. To account for heat losses, the radiative and convective heat transfer at the weld surface and the convective heat transfer to the cooling water and the surrounding air were modeled.

The overall heat flux was calculated as

$$\Phi = \eta E I \tag{2}$$

where η represents the efficiency factor, which accounts for radiative and other losses from the arc to the ambient environment, E is voltage and I electric current. The heat flux distribution in the material is defined by the equation

$$f(r,\Phi,z) = f_1 e^{-3\left[\left(\frac{r}{a}\right)^2+\left(\frac{\Phi r}{b}\right)^2+\left(\frac{z}{c}\right)^2\right]} \tag{3}$$

where r, ϕ, z are the radial, tangential and axial coordinates, respectively, with the origin at the material surface. Constants $2a$, $2b$ and $2c$ represent the characteristic arc dimensions in r, ϕ and z direction within which 95% of the energy is transferred. The constant f_1 can be derived by integrating the function $f(r, \phi, z)$ in the material half space beneath the welding arc ($-\infty < r < 0$, $-\infty < \phi < \infty$, $-\infty < z < \infty$):

$$f_1 = \eta E I \frac{1}{abc}\frac{6\sqrt{3}}{abc\pi\sqrt{\pi}} \tag{4}$$

Because the axisymmetric model was assumed, the dimension b does not physically exist. Therefore, the tangential dimension was simulated by adding the time component to the model:

$$\left(\frac{\Phi r}{b}\right)^2 = \left[\frac{v}{b}\left(t - \frac{t_t}{2}\right)\right]^2 \tag{5}$$

where t is the current time and t_t is the total time that the electrode needs to travel over the observed point, taking into account the actual welding speed, v (Table 1). Equation 3 combined with Equation 5 model the volumetric Gaussian distribution of heat flux by transferring the ϕ dimension of the axisymmetric model into the time dimension.

To model the conductive heat transfer, the thermal conductivity coefficients of both materials — SA210 and Alloy 625 — were given as a function of temperature. To account for heat transfer effects due to fluid flow in the weld pool, a linear increase in thermal conductivity by a factor of three between the melting temperature and 3000°C (5432°F) was assumed for both materials. Figure 3 shows the applied thermal conductivity for SA210 and Alloy 625.

The latent heat of fusion was specified to model the thermal effect of phase transformation. The value of 247 J/g was used for both materials (Ref. 9).

Calculation of the convection coeffi-

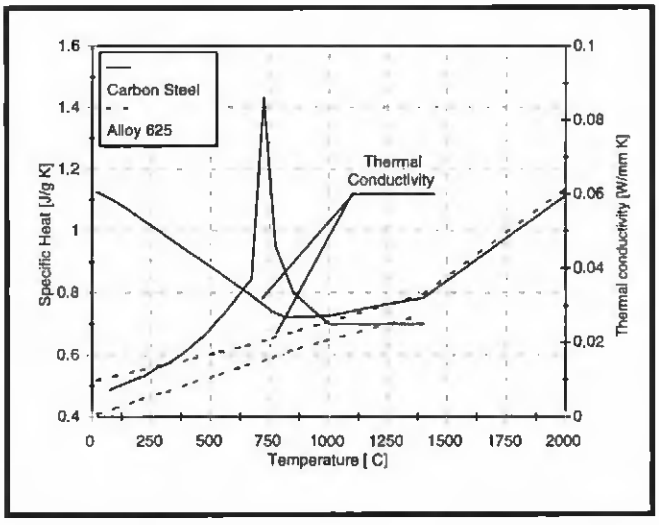

Fig. 3 — Specific heat and thermal conductivity for SA210 and Alloy 625.

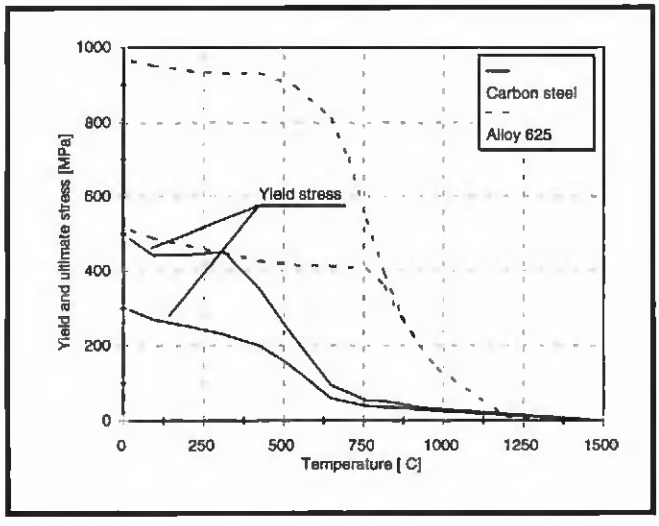

Fig. 4 — Yield and ultimate stress for SA210 and Alloy 625.

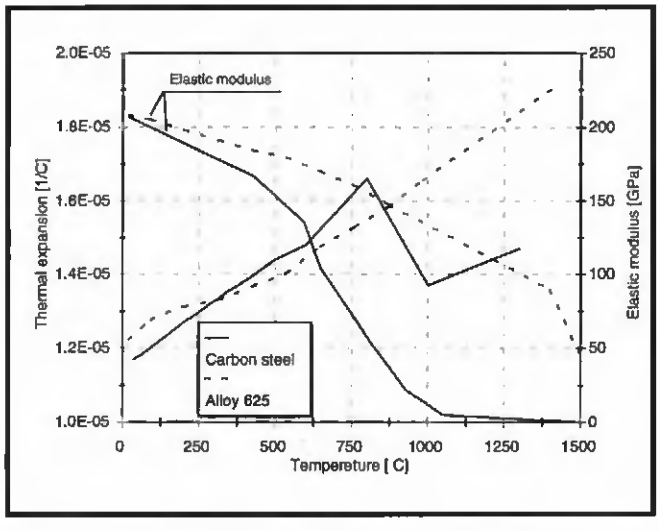

Fig. 5 — Thermal expansion and elastic modulus for SA210 and Alloy 625.

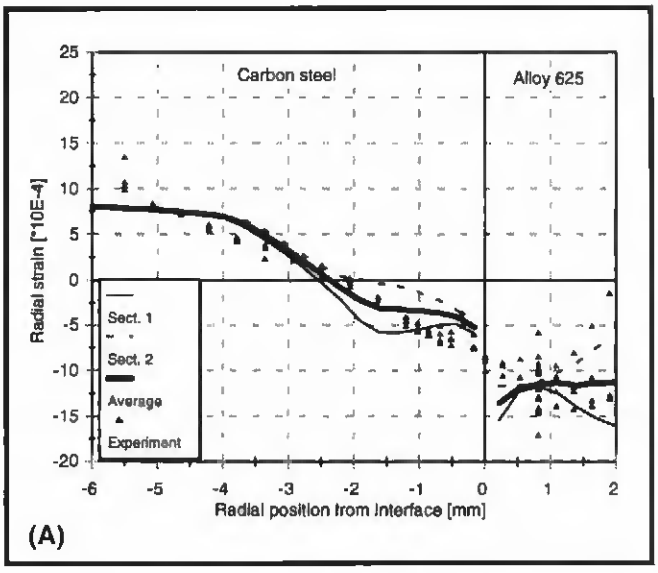

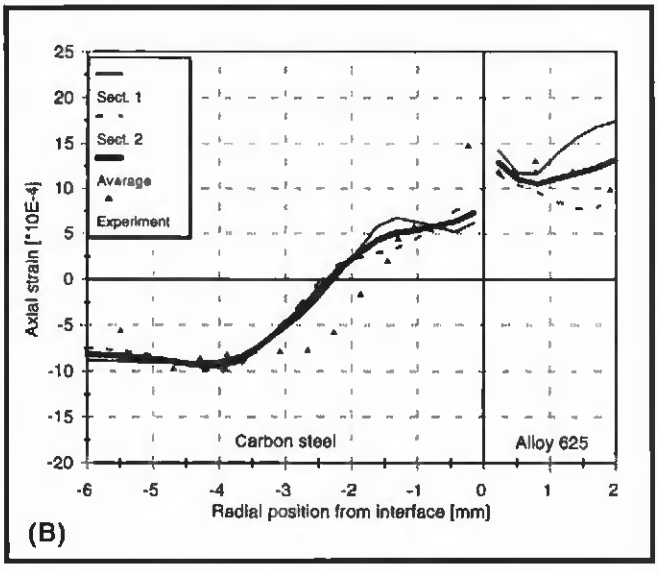

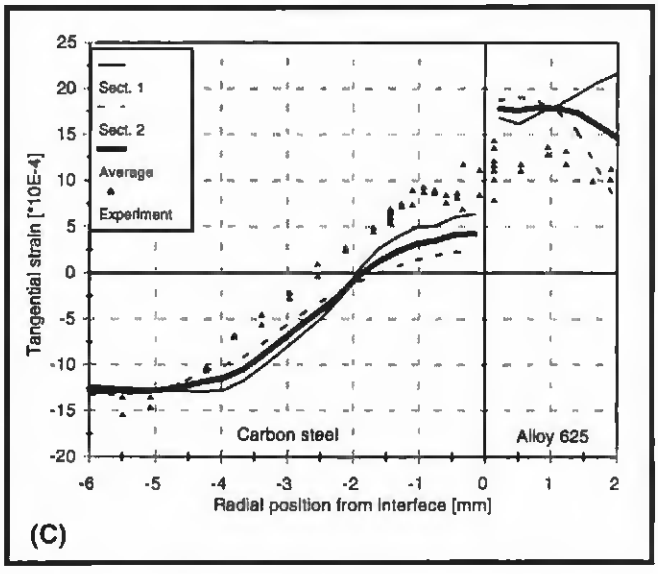

Fig. 6 — Comparison of elastic strain components (radial, axial, tangential) measured by ND and calculated by FE method.

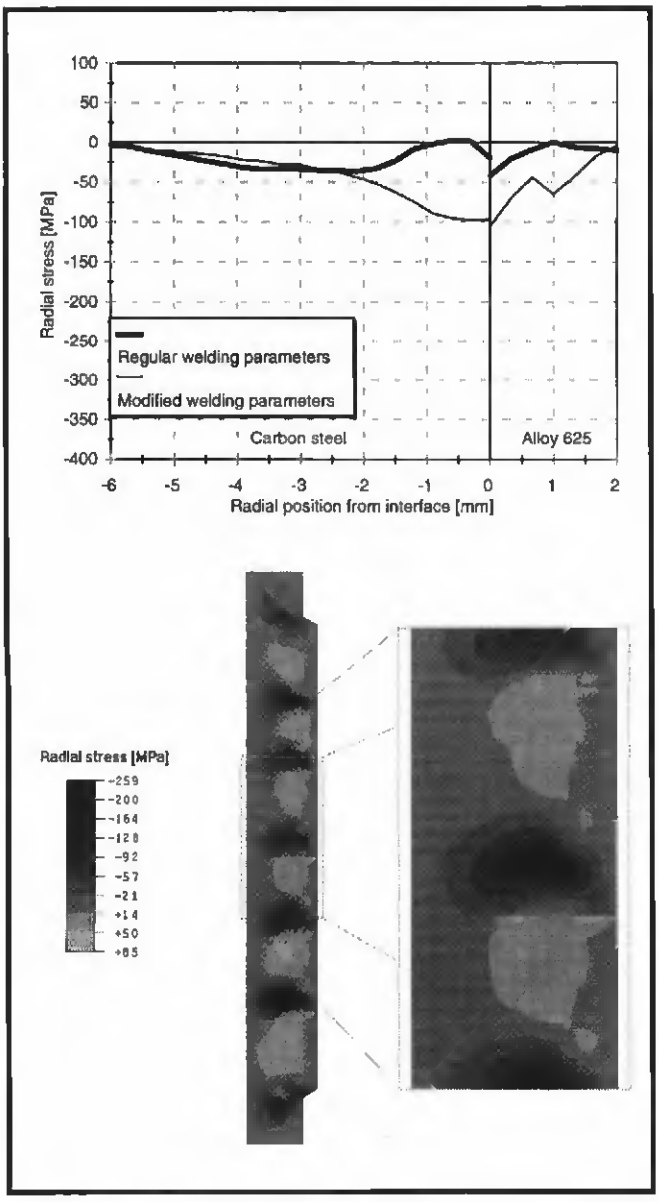

Fig. 7 — Radial residual stress.

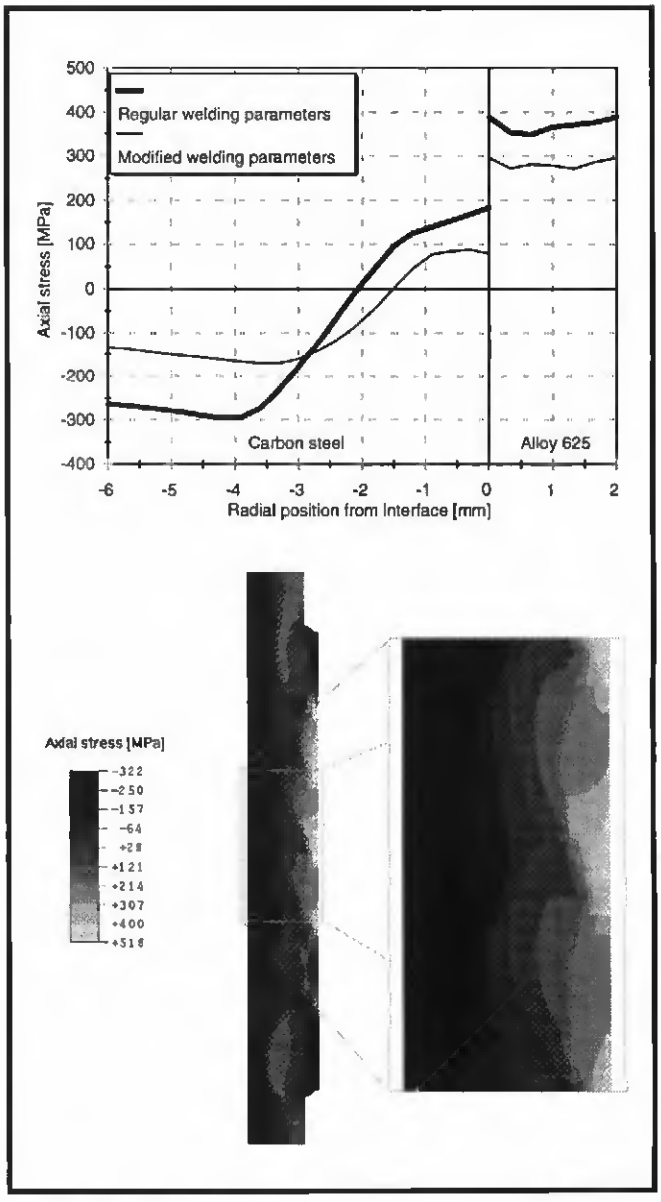

Fig. 8 — Axial residual stress.

cient, h_f, for convection to the cooling fluid was based on the water properties at 20°C (68°F) and the water flow rate in the tube is shown in Table 2. In addition, the tube-air convection coefficient, h_a, was calculated for the natural convection to the air of 20°C (68°F). Radiant heat transfer was assumed at the outside tube surface. The value of 0.2 was used for the emissivity coefficient.

Three computational steps are required to complete one welding pass. In the first step, the heat source passes across the observed section and heats/melts the tube material. The filler material is added in the second step. The third step, which is required because of the axisymmetric model assumption, simulates the cooling of the observed section before the electrode returns for the next welding pass. Because of the axisymmetric model assumption, the heat is simultaneously applied and the material is simultaneously melted and deposited around the circumference. The cooling in the third step undergoes the same assumption that creates sharp thermal cycles. To ensure more gradual heat distribution, which can better represent the continuous or progressive heat input in the circumferential direction in actual welding, additional heat is applied during the third step. The distributed heat flux, which equals the welding heat flux, is applied to the weld section of the tube during the cooling time. Six welding passes are simulated to obtain a weld of sufficient length and to get a uniform region of residual stresses that are unaffected by the beginning and end of the welding process. After the first layer is finished, the tube is cooled to room temperature, and then the second weld layer is started. The computational assumptions for the second layer are similar. Each welding pass for the second layer consists only of two computational steps — heating and cooling — because no filler material is to be added. After the last (sixth) pass of the second layer, the tube is again cooled to room temperature.

The heating time (first step) equals the time the electrode with the assumed diameter needs to travel across the observed point with the actual welding speed. The cooling time (third step) equals the time the electrode needs to travel around the tube, again with the actual trav-

eling speed specified in Table 1. The final cooling, which takes place after the second layer is finished (cooling after the sixth welding pass), lasts until the tube reaches the isothermal ambient temperature.

Mechanical Analysis

An elasto-plastic constitutive law was used in the mechanical analysis. The temperature-dependent mechanical properties were obtained elsewhere (Refs. 10–13). Figure 4 shows the temperature-dependent yield and ultimate stresses for 5A210 and Alloy 625. Both yield and ultimate stresses were reduced to 10 MPa at the melting temperature to simulate the low strength at high temperatures. Elastic modulus was also given as a function of temperature and reduced to a small value (5000 MPa) at high temperatures — Fig. 5. The Poisson's ratio of SA210, which has the value of 0.28 at room temperature, increases linearly to 0.3 at 430°C (806°F) and is constant for higher temperatures. The Poisson's ratio of Alloy 625 is 0.28 at room temperature and linearly increases to 0.33 at 1280°C (2336°F). Phase transformation effects due to rapid cooling on mechanical properties of carbon steel were not included in the analysis.

The same FE mesh was used as in the thermal analysis. The analysis is based on the temperature gradients calculated in the thermal analysis, which represents the input information, or loading. The tube was not restrained during mechanical analysis because it is rotating and simultaneously moving in the axial direction during the actual welding process.

Residual stresses and elastic strains were calculated after the welding process was completed and the tube had cooled to room temperature. Residual elastic strains were evaluated for comparison with the ND results. The purpose of the comparison is to validate the FE model, which will be discussed in the following section.

Results and Discussion

Verification of the FE model

The analysis was verified by comparing the calculated elastic strains to those measured by the ND technique. Because the elastic strains were directly measured by ND, their comparison to FE elastic strains avoids the error from conversion to stress values (Ref. 3). Residual elastic strains were measured in three directions — radial, axial and tangential. These strains were then used to determine the accuracy of the FE model. Figure 6 shows the comparison. Note that the FE results are presented in two through-thickness sections. Section line 1 is located between the two weld passes, and section line 2 is at the center of the weld pass where the highest stress variation occurred — Fig. 2. Also note that the ND results were measured across several weld passes (radial and tangential components), and therefore represent an average strain.

Based on the results presented in Fig. 6, it can be concluded that the agreement in axial and radial directions is excellent. The calculated and measured tangential strains at the inner tube surface agree well. In other areas, however, the calculated tangential strains are consistently higher. This may be explained by the macroscopic model nature, which prevents capture of the micro effects at the interface between the two materials during deposition, solidification and cooling transients. This may be in accord with dilution shown after removal of the carbon steel material. Conversely, one may use the good agreement in radial and axial strain components to disprove the significance of the above-mentioned effects on the FE stress-strain results. However, the overestimation in tangential component could also be explained as follows. The axisymmetric model assumption means that the material deposition around the circumference is made simultaneously. Because the circular layer of material is at high temperature during deposition on the tube, which is at room temperature, considerable shrinkage of the deposited layer occurs when the composite is cooled to room temperature. This creates tensile stresses in the cladding and compressive stresses in the base material. The difference in thermal expansion coefficients also affects the magnitude of the resulting stresses. The physics of gradual deposition in the circumferential direction may have different effects on shrinkage because the deposited material cools while the welding is still in progress. Intuition suggests that the tangential shrinkage may not be as intense in the case of continuous-progressive solidification and cooling in the circumferential direction (actual welding process) compared to the simultaneous weld solidification and cooling of the entire circumference (axisymmetric model). This might contribute to the higher stress magnitude in the tangential direction.

Residual Stresses

Residual stresses and strains were evaluated after the welding process was completed and the tube had cooled to room temperature. The calculated residual stresses along the two section lines were averaged and presented for radial, axial and tangential direction in Figs. 7–9, respectively. A shaded cross-section plot is added to each figure to show the stress pattern. The results for equivalent plastic strain are also presented in Fig. 10. The section line 1 intersects the tube between the third and the fourth weld pass, whereas the section line 2 intersects it in the middle of the fourth pass — Fig. 2. Sections were selected to capture the two extremes in the through-thickness stresses and strains. The two middle passes were evaluated to minimize the beginning and end weld effects on the stress distribution, which are shown in shaded plots of Figs. 7–10.

Averaged radial stresses are compressive and their magnitude is not significant (up to 50 MPa), as shown in Fig. 7. The stress pattern is unique in that the stresses underneath each weld pass are tensile, whereas they are compressive underneath the interface between the two weld passes as shown in the shaded plot of Fig. 7.

Axial residual stresses in the weld cladding are tensile and lower than the yield stress. The calculated average stress is between 350 and 400 MPa. Stresses in the carbon steel are tensile at the interface (200 MPa), decrease to about a 300-MPa compressive stress at approximately one-third of the tube thickness, and remain constant to the inner surface — Fig. 8.

Figure 9 shows that the calculated tangential residual stress distribution is similar. Stresses in the cladding and in the carbon steel core are higher by about 100 MPa, compared to the axial stress. According to the explanation given in the previous section, the tangential stresses are expected to overestimate the actual value.

The FE results also show that the whole tube was plastically deformed during the welding process. The highest plastic strain occurred at the interface (up to 0.18). It is lower at the inner tube surface (approximately 0.02), but higher in the weld cladding (approximately 0.08) — Fig. 10. The calculated plastic strains may overestimate the actual value because in the FE analysis the strains accumulate over the heating and cooling transients.

In general, residual stresses in the weld cladding and at the interface of the two materials are high and tensile, which is important information for evaluating the clad tube with respect to potential failure mechanisms.

Two processes were considered to prevent or reduce the tensile residual stresses in the weld cladding. First, the

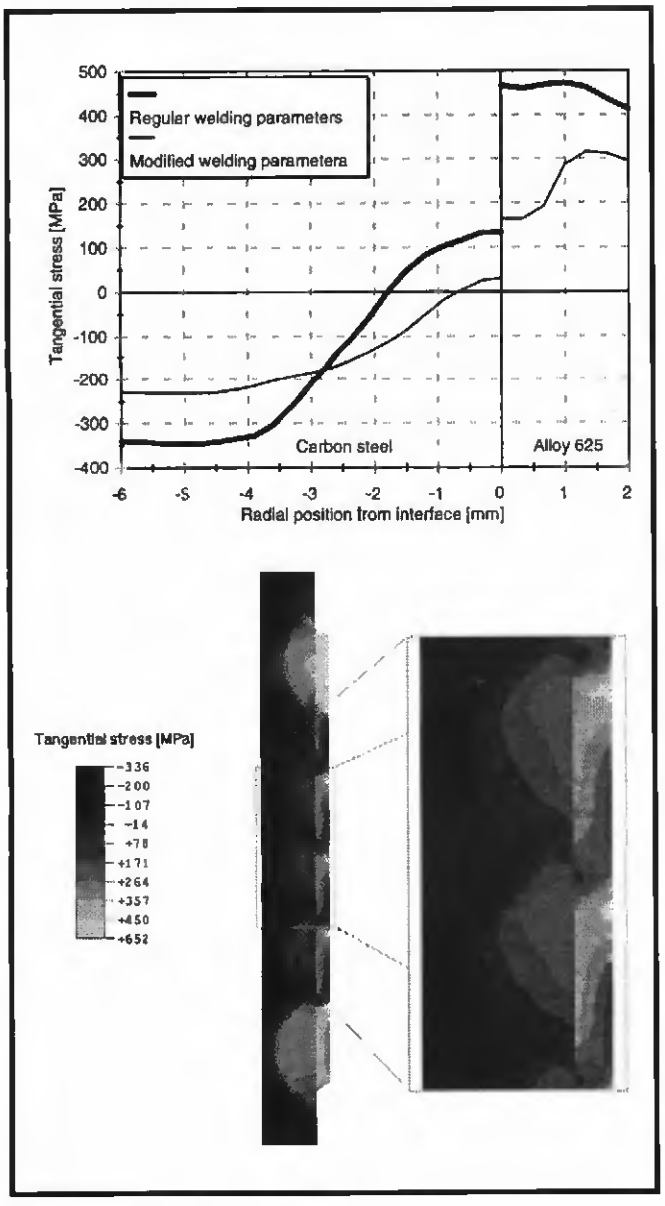

Fig. 9 — Tangential residual stress.

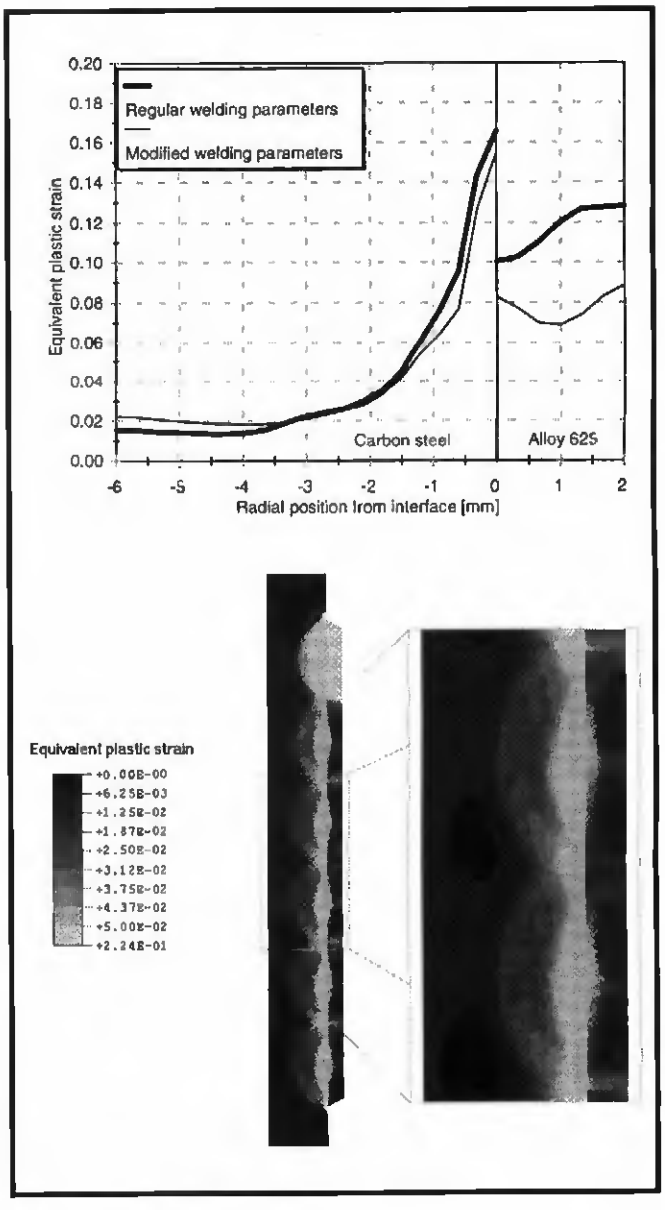

Fig. 10 — Equivalent plastic strain.

welding process was modified so that the water cooling was removed and a preheat of 93.3°C (200°F) was applied. Next, the heat input for the second layer was reduced by lowering the electric current from 400 to 250 A. As a result, the average radial stresses are higher (up to 100 MPa), but the axial and tangential stresses are considerably lower. In the carbon steel core they are lower for approximately 100 MPa. The same applies to axial stresses in the weld cladding, whereas the tangential stresses in the weld cladding are lower for 100 to 300 MPa. Figures 7–10 show the results.

Annealing after the welding at 900°C (1652°F) for 20 min was even more successful in relieving the residual stresses. The residual stresses after the heat treatment were reduced to almost zero (Ref. 8). Figure 11 shows the comparison of the tangential strains in the as-manufactured tube and the annealed tube.

Stresses at In-Service Conditions

Due to the importance of in-service stresses for evaluation of various cracking mechanisms for the tubes in black liquor recovery boilers, the stress state was also analyzed at the operating conditions, with a uniform temperature of 287°C (549°F) and internal pressurization of 8.62 MPa. The in-service stresses in the tubes made by the regular welding process (welding parameters defined in Table 1) and the modified welding process as discussed in the previous section, do not change significantly from their residual stresses. The axial stresses are approximately 50 MPa lower throughout the tube thickness, whereas the tangential stresses are lower for approximately 50 MPa only at the inner surface. The change in radial stresses is negligible. Note that the performed analysis took into account only the residual stresses due to the weld cladding process, and the residual stress state shall be different after the panel assembly. However, the discussed results give an answer on the magnitude of the in-service stresses relative to the magnitude of residual stresses in the tube. Stresses in the annealed tube — assumed zero residual stress — at the operating conditions reach the magnitude of about 30 MPa.

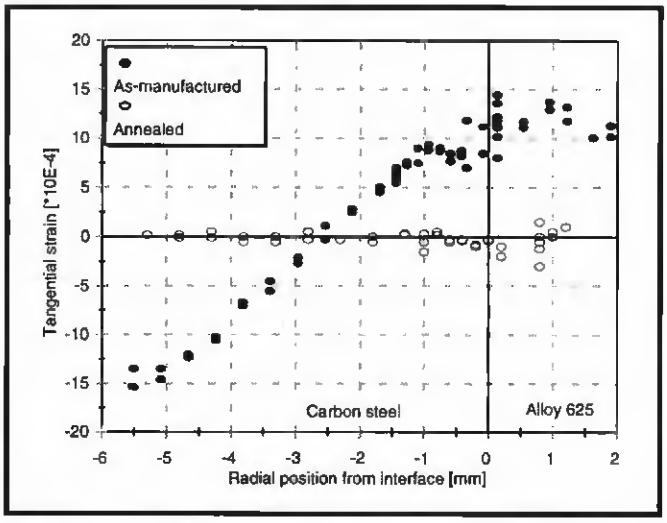

Fig. 11 — Measured tangential strains for as-manufactured and annealed tube.

The reason for such a small stress difference between the as-manufactured tube and the tube at the operating conditions is due to the small difference in the thermal expansion coefficients between the two tube materials — Fig. 5.

Conclusions

In this study, an axisymmetric FE model was developed for the simulation of the spiral weld cladding process. The residual stress and strain distributions in the weld clad tube were analyzed. The residual elastic strain distribution was measured using the ND technique in a parallel study (Ref. 8). The measured data were used to verify the developed FE model. Excellent agreement in radial and axial elastic strain components was obtained, while the calculated tangential strains overestimated the measured values. The disagreement in the tangential component, which may result from the simplification of the welding process with an axisymmetric model, is discussed in this paper.

The calculated axial stresses in the weld cladding are very high and tensile, with an average of 375 MPa. They are compressive and of lower magnitude at the inner tube surface. The calculated tangential stresses in the cladding are tensile and also very high, with an average of 450 MPa. The comparison of measured and calculated elastic strains suggests that the calculated tangential stress component, especially in the weld cladding, is higher than the actual stress. Radial stresses are mainly compressive, and their magnitude is not significant compared to the axial and tangential stress components.

The analysis shows that the whole section — tube and weld — undergoes plastic deformation during welding. The plastic strain is the highest at the interface and in the weld cladding.

The results show that modifications to the current welding process, *i.e.*, removal of cooling water, application of preheat and reducing the electric current of the second layer, affect the residual stresses in the clad tube. The average axial and tangential stresses in the carbon steel core and in the cladding are lower for approximately 100 MPa.

Annealing the welded tube at 900°C (1652°F) relieves the residual stresses to almost zero.

Stresses in the tubes at the operating conditions do not change significantly from their residual stress state.

In general, the results obtained in this study are very promising for determining the residual stress patterns of complex welding processes by a FE model. The developed model can be used in a future parametric sensitivity study to analyze the effect of various welding parameters on the residual stress distribution.

Acknowledgments

The authors would like to thank Dr. Yaoshan Chen and Dr. Andrew Payzant for reviewing this paper. The research was sponsored in part by an appointment to the ORNL Postgraduate Research Associates Program administered jointly by the Oak Ridge Institute for Science and Education and ORNL. The research was also sponsored by the U.S. Department of Energy, Assistant Secretary for Energy Efficiency and Renewable Energy, Office of Industrial Technologies, Advanced Industrial Materials Program, under contract DE-AC05-96OR22464 with Lockheed Martin Energy Research Corp.

References

1. Singbeil, D. L., Prescott, R., Keiser, J. R., and Swindeman, R. W. 1996. Composite tube cracking in Kraft recovery boilers. Draft technical report, Pulp and Paper Institute of Canada.

2. Keiser, J. R., Taljat, B., Wang, X.-L., Maziasz, P. J., Hubbard, C. R., Swindeman, R. W., Singheil, D. L., and Prescott, R. 1996. Analysis of composite tube cracking in recovery boiler composite floors. *Proceedings of 1996 TAPPI Engineering Conference*, Chicago Ill.

3. Mahin, K. W., Winters, W., Holden, T. M., Hosbons, R. R., and MacEwen, S. R. 1991. Prediction and measurement of residual elastic strain distributions in gas tungsten arc welds. *Welding Journal*, 70(9): 245-s to 254-s, Sep. 1991.

4. Roelens, J. B. 1996. Numerical simulation of some multipass submerged arc welding determination of the residual stresses and comparison with experimental measurements. *The Eighth International Conference on Pressure Vessel Technology*, Montreal, Canada.

5. Jovanovic, A., and Lucia, A. C. 1986. Analysis of cladding residual stresses and their influence on the structural reliability of LWR pressure vessels. *Int. J. Pressure Vessels Piping*. 22: 111–145.

6. Teraski, T., Akiyama, T., Ishimura, T. 1995. New method for estimating residual stresses in pipe made by surfacing weld. *Eng. Ind.* 117: 365–371.

7. ABAQUS, 1996 *Users' Manual*, Version 5.5. Hibbitt, Karlson & Sorensen.

8. Wang, X.-L., Payzant, E. A., Taljat, B., Hubbard, C. R., Keiser, J. R., and Jirinec, M. J. 1996. Experimental determination of the residual stresses in a spiral weld overlay tuhe. *Mater. Sci. Eng. A*.

9. Touloukian, Y. S., and Ho, C. Y. 1981. *Properties of Selected Ferrous Alloying Elements*. Vol. 3, McGraw-Hill Book Company.

10. Swindeman, R. W. 1996. A review of thermal/mechanical fatigue in composite tube materials. Draft technical report, Lockheed Martin Energy Research Corp., Oak Ridge National Laboratory.

11. Boyer, H. E., and Gall, T. L. 1992. *ASM Metals Handbook*, Desk Edition, ASM International, Metals Park, Ohio.

12. Rothman, M. F. 1989. *High Temperature Property Data: Ferrous Alloys*. ASM International, Metals Park, Ohio.

13. Smith, G. V. 1970. *An Evaluation of the Elevated Temperature Tensile and Creep-Rupture Properties of Wrought Carbon Steel*. ASTM, Philadelphia, Pa.